Comparison of ray and full-wave synthetic seismograms of reflected SH waves in attenuating media

Ivan Pšenčík [1,4], Miłosz Wcisło [2,3] and José Carcione [5]

[1]Institute of Geophysics, Acad. Sci. of CR, Boční II, 141 31 Praha 4, Czech Republic. E-mail: ip@ig.cas.cz
[2]Institute of Rock Structure and Mechanics, Acad.Sci. of the CR, V Holešovičkách 41, 182 09, Praha 8, Czech Republic. E-mail: wcislo@irsm.cas.cz
[3]Faculty of Mathematics and Physics, Department of Geophysics, Charles University, V Holešovičkách 2/747, 180 00 Praha 8, Czech Republic
[4]Faculty of Mathematics and Physics, Department of Geophysics, Charles University, Ke Karlovu 3, 121 16 Praha 2, Czech Republic
[5]Istituto Nazionale di Oceanografia e di Geofisica Sperimentale (OGS), Borgo Grotta Gigante 42c, I-34010 Sgonico, Trieste, Italy. E-mail: jcarcione@inogs.it

Summary

We evaluate accuracy of approximate ray computations in anelastic media by comparing ray synthetic seismograms of an SH wave reflected at a horizontal interface separating two homogeneous, isotropic, elastic or anelastic half-spaces with full-wave synthetic seismograms. The comparison shows good accuracy of ray results outside the critical region of a reference elastic model. In the critical region, the ray method does not work properly anyway. The comparison confirms conclusions of previous studies showing that the effects of attenuation on reflection and transmission coefficients are insignificant in comparison with effects of attenuation on wave propagation. Use of a non-causal attenuation instead of a causal one leads to more significant distortions.

Introduction

We test the accuracy of the weak attenuation concept (WAC). WAC is a perturbation technique, in which attenuation is considered as a perturbation of the reference elastic state. In this way, it allows an approximate evaluation of the effects of attenuation on seismic-wave propagation. The concept was proposed by Kravtsov and Orlov (1990), in original version already in the eighties. Its use in the study of effects of attenuation inside layers by Moczo et al. (1987) or Gajewski and Pšenčík (1992), and its extension to the study of effects of attenuation on reflection/transmission process by Pšenčík et al., (2022) showed that WAC, although designed for weak attenuation, is applicable to attenuation encountered in most seismological studies. In this study, we test the accuracy of WAC implemented to the programme package SEIS (Červený and Pšenčík, 1984) designed for 2D computations of seismic wavefields in isotropic layered structures with laterally varying velocities. The reflection and transmission coefficients in the modified SEIS package are

Seismic Waves in Complex 3–D Structures, **31** (2022), 55–68 (ISSN 2336–3827, online at http://sw3d.cz)

computed so that the propagation vector of the transmitted wave in the overcritical region is forced to behave physically, i.e., to point to the bottom half-space, see detailed discussion of this phenomenon by Pšenčík et al., (2022). Let us mention that the above enforcement leads to the violation of some constraint relations, under which the reflection and transmission coefficients were derived.

For the tests, we use the seismograms of an SH wave reflected at an interface separating two homogeneous, isotropic elastic and anelastic half-spaces. We compare the SH-wave ray seismograms generated by the modified SEIS package with the full-wave (PS) synthetic seismograms computed by the procedure based on the Fourier and Chebyshev pseudospectral methods to compute the spatial derivatives. The procedure is called domain decomposition in computational acoustics. It has been used extensively to model elastic and electromagnetic waves (Carcione and Helle, 2004; Carcione et al., 2006). The upper and bottom half-spaces are covered by grids. The solution on each grid is obtained by using the Runge-Kutta method as a time-stepping algorithm and the Fourier and Chebyshev differential operators to compute the spatial derivatives (Carcione, 2014). The method, which implements the boundary conditions explicitly, has been verified extensively (Sidler and Carcione, 2007; Sidler et al. 2008; Ursin et al. 2017). PS modelling can be considered exact within the limits of computer precision, and when the temporal and spatial discretization is chosen properly to avoid aliasing and numerical dispersion.

Model, configuration, source and the attenuation type

The model used for testing consists of two half-spaces separated by a horizontal interface, see Figure 1. Each half-space is specified by the S-wave velocity β_i, the density

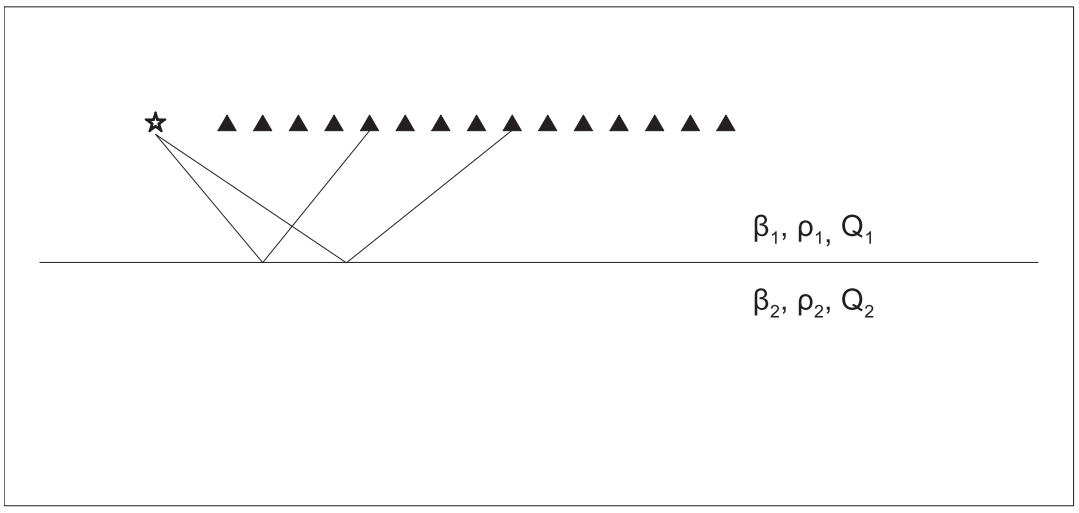

Figure 1: Model and configuration used in tests. The depth of the reflector below the source-receiver profile is 0.248 km. Parameters of the half-spaces are given in Table 1.

Model	β_1(km/s)	β_2(km/s)	$\rho_1(g/cm^3)$	$\rho_2(g/cm^3)$	Q_1	Q_2
M1 (EL/EL)	2.0	2.8	2.4	1.5	∞	∞
M2 (EL/AN)	2.0	2.8	2.4	1.5	∞	60
M3 (AN/AN)	2.0	2.8	2.4	1.5	40	60

Table 1: Parameters of models used in tests. β - S-wave velocity, ρ - density, Q - quality factor.

ρ_i and the quality factor Q_i, $i = 1, 2$. The source and a set of receivers are all distributed along a horizontal profile in the upper half-space. No free-surface effects are considered at receivers. The offset of the first receiver from the source is 0.005 km, the separation of receivers is 0.02 km. The reflector is situated at a depth of 0.248 km below the receiver profile. Three models are considered. In model M1, the upper and bottom half-spaces are elastic (EL). In model M2, upper half-space is elastic (EL) and the bottom half-space is anelastic (AN). In third model, M3, both half-spaces are anelastic (AN). As shown in Table 1, S-wave velocities β_i and the densities ρ_i are the same in all three models. S-wave velocities are chosen so that they guarantee the existence of a critical reflection in the reference elastic model, which is in our case model M1. For the above-chosen configuration and S-wave velocities, the offset of the critical point is 0.506 km. In order to make models as simple as possible, the densities are chosen so that the incidence of a wave at the reflector under the Brewster angle is avoided.

A point source with unit radiation pattern and Ricker signal as the source-time function are used. In 2D models, Ricker signal loses its symmetry and has a slowly decaying tail (this is the consequence of the fact that the signal is the time convolution of the wavelet and two-dimensional Green function). In model M1, the resulting signal has the form shown in Figure 2. It shows the signal generated in the PS code (red) overlaid by its ray counterpart (black) generated in the modified SEIS programme package. Instead

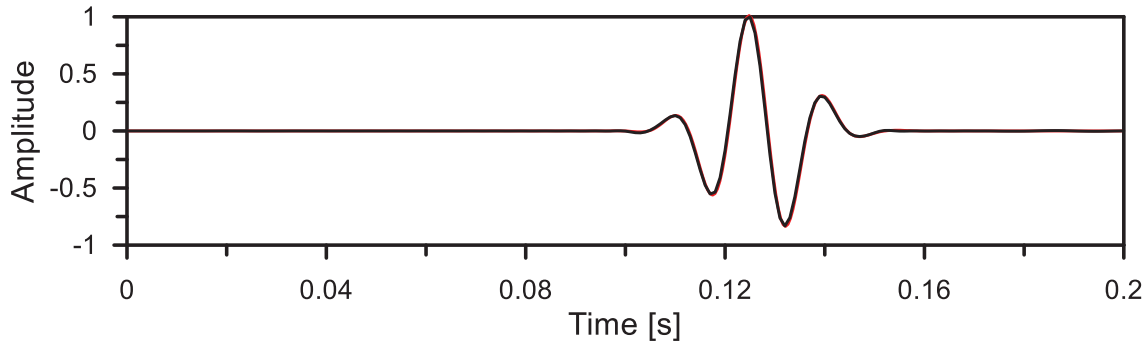

Figure 2: The signal resulting from the convolution of the Ricker signal with 2D Green function used in the PS code (red) overlaid by its ray counterpart (black) used in the modified SEIS programme package.

of introducing 2D Green function to the SEIS package, we decided for the following procedure (note that Klimeš, 2021 had to solve a similar problem). We digitized the PS direct-wave arrival and used the table of resulting values as an input for the SEIS

package (SEIS package allows such an option). Figure 2 shows that the fit of direct waves generated by the modified SEIS package (black) and by the PS code (red) and SEIS package is perfect. This waveform is used in all following computations as an input signal.

For the description of the attenuation effects, Maxwell dissipation model is used. Note that this model represents a special case of Müller dissipation model (Müller, 1983; see also Červený, 2001). In Maxwell dissipation model, for $Q \gg 1$ we have:

$$\beta^{-1}(\omega) \sim \beta^{-1}(\omega_0)\Big(1 + \frac{\mathrm{i}}{2Q(\omega)}\Big) \ , \qquad Q(\omega) = Q(\omega_0)\omega/\omega_0 \ . \tag{1}$$

The plus sign in equation (1) corresponds to the used form of the exponential factor of the time-harmonic plane waves: $\exp[-\mathrm{i}\omega(t - p_k x_k)]$. Here ω is the circular frequency and ω_0 is the reference frequency. Unless specified otherwise, causal attenuation is considered.

Tests

In the following plots, we present comparisons of PS (exact) SH-wave seismograms (red) overlaid by SH-wave ray seismograms (black). Real amplitudes with the same scaling factor are used in Figures 3-5.

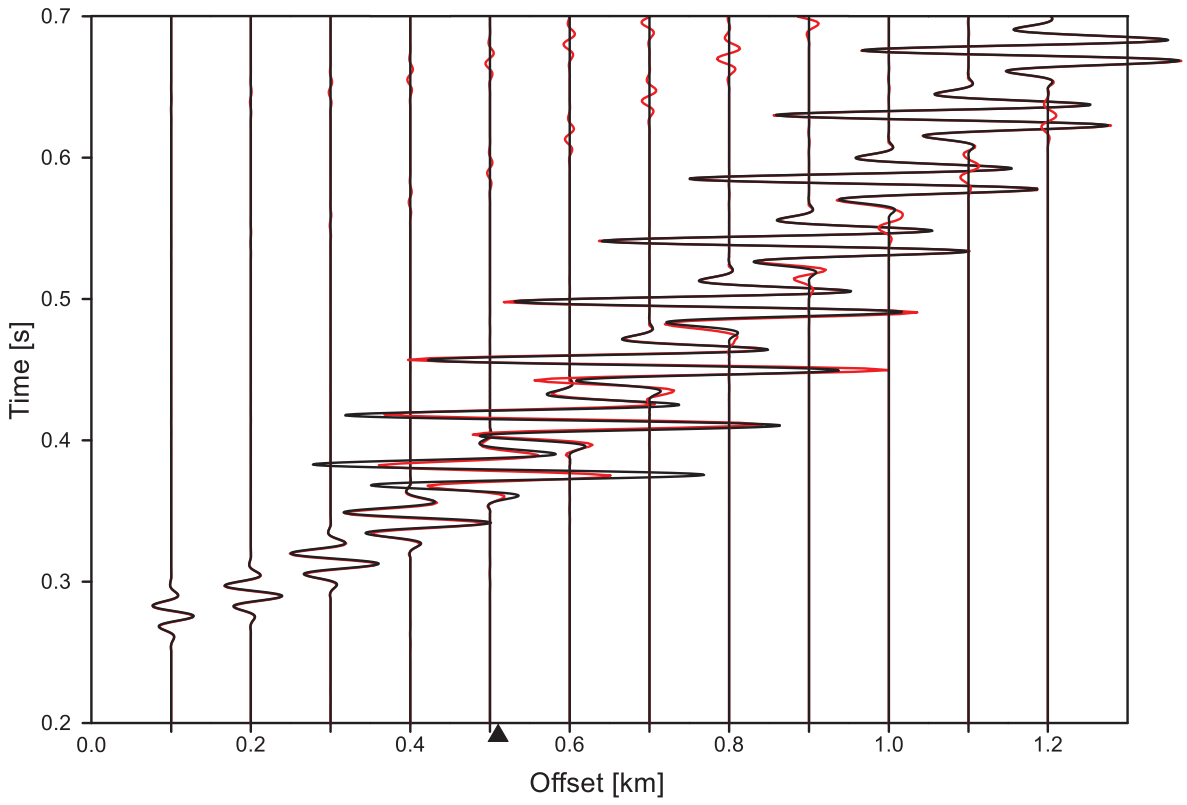

Figure 3: PS seismograms (red) overlaid by ray seismograms (black) in model M1 (EL/EL). Full triangle indicates the position of the critical point. Red arrival preceding the reflection behind the critical point is the head wave. Later red arrivals are numerical errors of the PS method.

Seismograms in Figure 3 correspond to model M1 composed of two elastic half-spaces (EL/EL). The section can be divided to the subcritical (below the offset of 0.506 km) and overcritical (above the offset of 0.506 km) parts. We can observe a perfect fit of ray and PS seismograms indicated by nearly missing red colour of PS seismograms. Some (red) disturbances can observed as later arrivals behind the reflected wave. These are "ghost" waves caused by numerical errors in the PS computations. Differences between ray and PS synthetic seismograms are negligible in the subcritical region. In the overcritical region, we can observe some other differences. They are caused by the head wave, which is correctly calculated in the PS seismograms, but missing in ray results. The missing head wave causes differences in waveforms immediately behind the critical point. For offsets larger than 0.9 km, the head wave starts to separate from the reflected wave and appears in the first arrival. As expected, greatest deviations between PS and ray seismograms are in the critical region. It is because the ray method does not work in this region properly. It yields greater amplitudes than correct. Seismograms computed for larger offsets are not shown here. The reason is the fact that waveforms of reflected waves generated by both codes at larger offsets are practically identical. The only difference is the head wave appearing in the PS results, which is missing in ray results. Comparison of ray and PS seismograms in Figure 3 serves as a reference for comparisons of seismograms affected by attenuation.

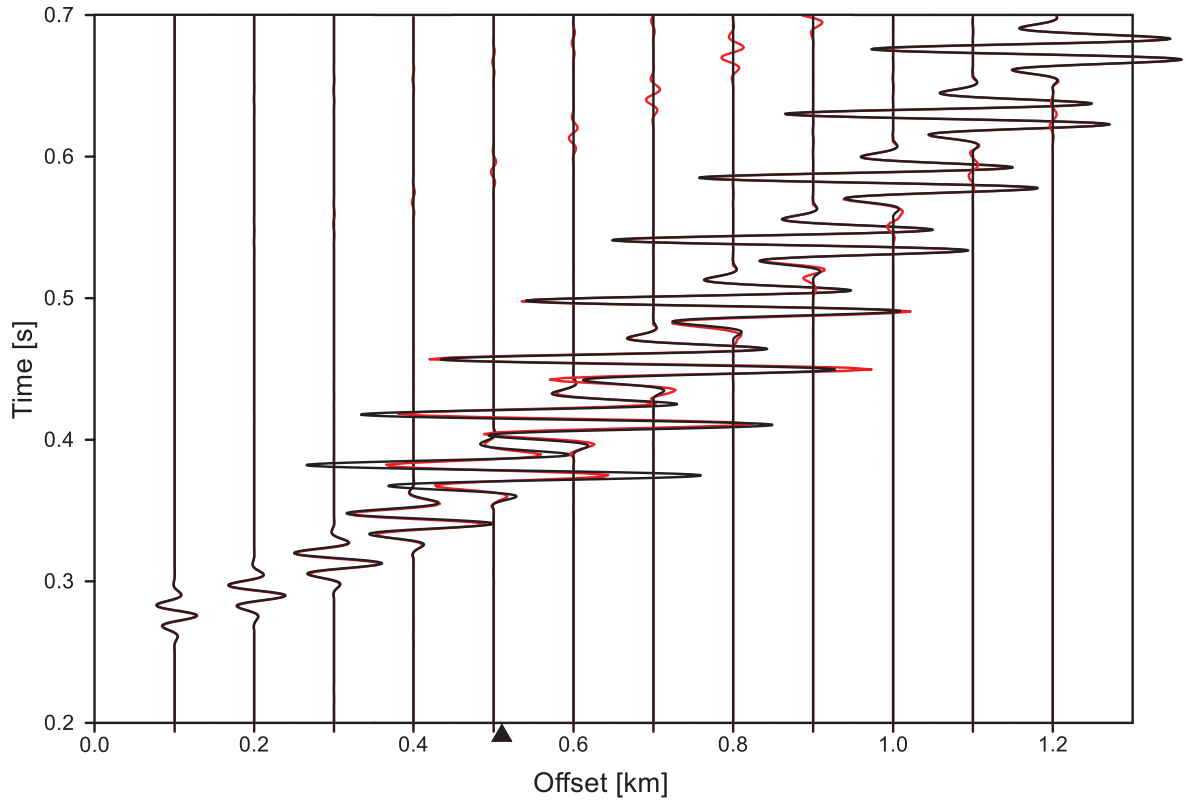

Figure 4: PS seismograms (red) overlaid by ray seismograms (black) in model M2 (EL/AN). Full triangle indicates the position of the critical point in model M1. Red arrival preceding the reflection behind the critical point is the head wave. Later red arrivals are numerical errors of the PS method.

Seismograms compared in Figure 4 are generated in model M2 (EL/AN), in which the upper half-space remains elastic and the bottom half-space is anelastic. For values of parameters see Table 1. The only way how attenuation can affect seismograms in model M2 is at the reflection point. Since Pšenčík et al., (2022) showed that the effect of attenuation on the reflection/transmission process is considerably smaller than on the wave propagation, it is no surprise to observe that seismograms in Figure 4 do not differ much from seismograms in Figure 3. Very small differences can be observed in the critical region, in which the ray results are unacceptable anyway. Comparison of Figures 3 and 4 indicates that Gajewski and Pšenčík (1992) did not make a significant mistake when they ignored effects of attenuation on the reflection/transmission in their study.

Figure 5 shows the comparison of PS and ray seismograms in model M3 (AN/AN) with both half-spaces attenuating. Due to significant effects of attenuation on the propagation of the wave in the upper half-space, amplitudes of seismograms in Figure 5 are significantly smaller than in Figures 3 and 4. As in previous figures, we can observe perfect (even better) fit of PS and ray seismograms outside the critical region. We can see that attenuation suppressed the "ghost" waves generated in the PS code and also reduced amplitudes of head waves, which are hardly observable.

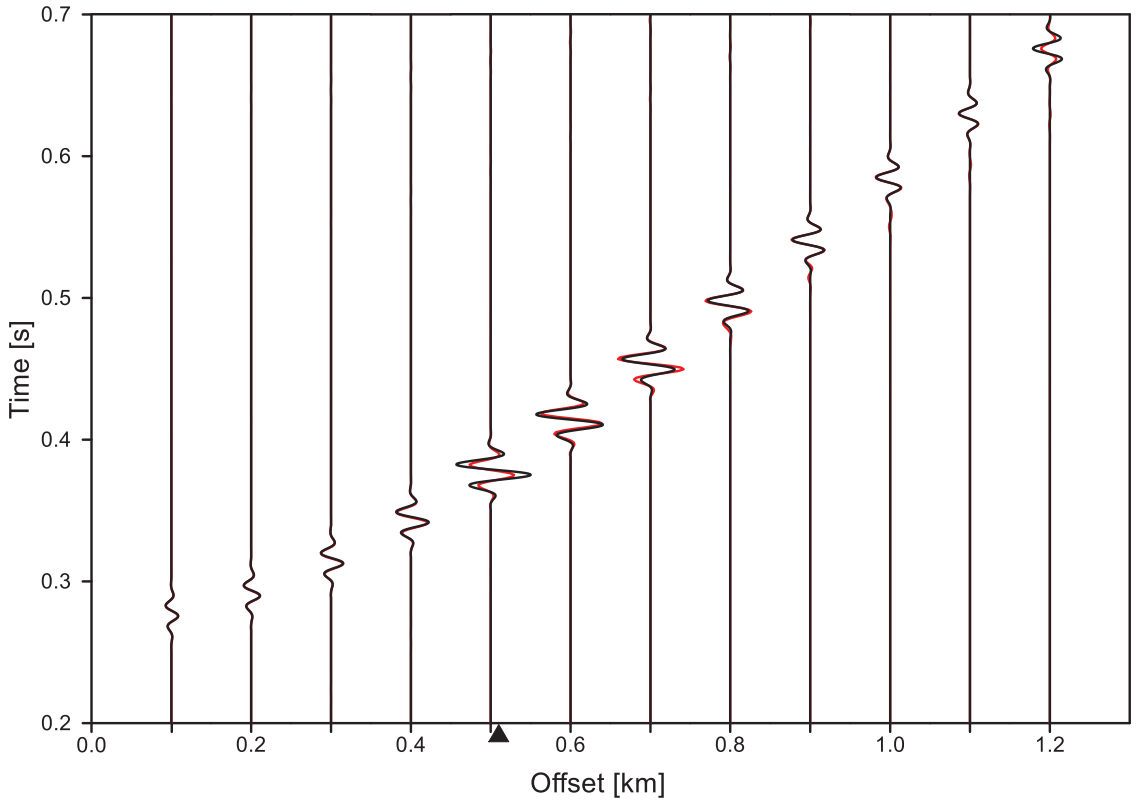

Figure 5: PS seismograms (red) overlaid by ray seismograms (black) in model M3 (AN/AN). Full triangle indicates the position of the critical point in model M1. Red arrival preceding the reflection behind the critical point is the head wave. Later red arrivals are numerical errors of the PS method.

In order to increase visibility of details in the following tests, Figure 6 shows the same seismograms as in Figure 5, but with doubled amplitudes. Head wave hardly visible in

Figure 5 is better visible, "ghost waves" are nearly invisible. In the following we use ray seismograms from Figure 6 as a reference (red) in comparisons, in which various effects of attenuation are investigated.

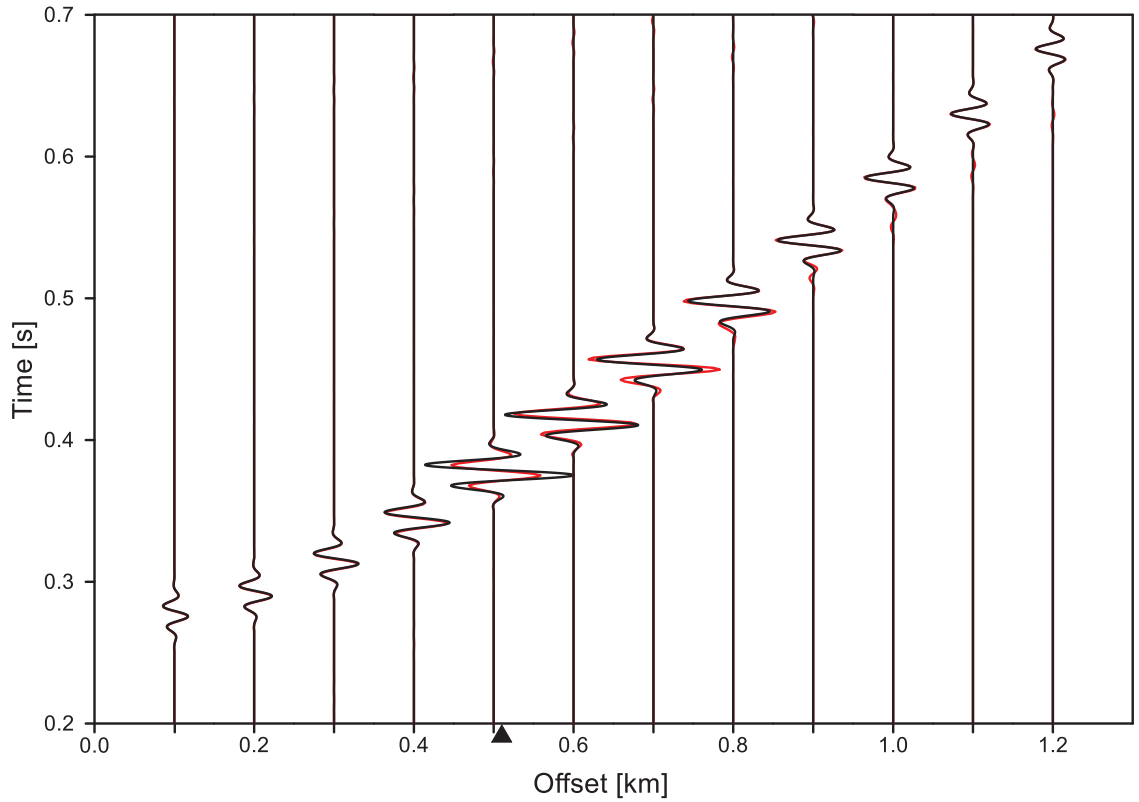

Figure 6: PS seismograms (red) overlaid by ray seismograms (black) in model M3 (AN/AN) (as in Figure 5) with doubled amplitudes.

In Figure 7, one can see ray seismograms from Figure 6 overlaid by ray seismograms, in which effects of attenuation on the reflection/transmission are ignored (black). In the subcritical region the differences are invisible, in the overcritical region, neglection of attenuation effects on reflection coefficient leads to a minor decrease of amplitudes close to the critical point. With increasing offset the differences between red and black seismograms diminish. We can see once again, that effects of attenuation on reflection/transmission play a negligible role.

In Figure 8, we check consequences of the removal of the enforced orientation of the propagation vector of the transmitted wave in the overcritical region so that it points to the bottom half-space. Pšenčík et al. (2022) have shown that this leads to the distorted forms of reflection and transmission coefficients (see their Figures 6 and 8) mostly in the critical region. Comparison of seismograms with enforced orientation (red) and with removed enforcement (black) in Figure 8 shows that the effect on seismograms is less pronounced than on coefficients themselves. In fact, the effects are comparable with complete removal of effects of attenuation on the reflection coefficient as can be seen in Figure 7. Ignoring effects of attenuation on the reflection and transmission coefficients does not seem to lead to significant loss of accuracy.

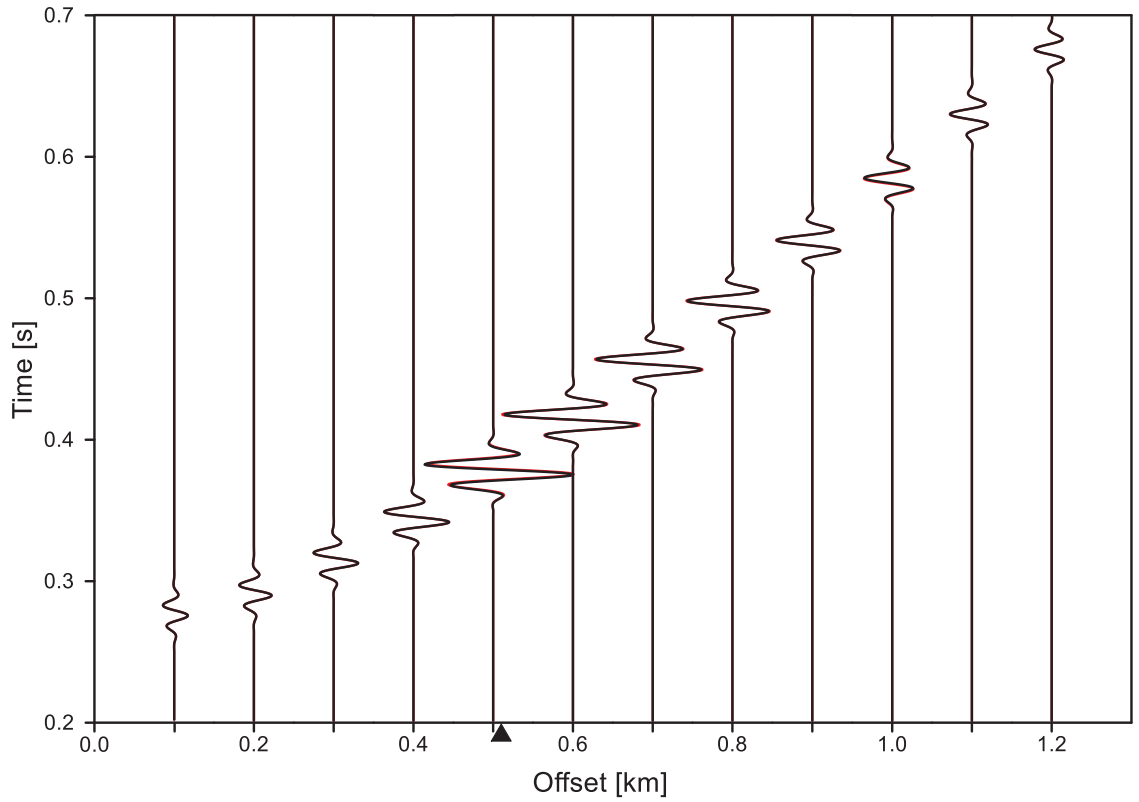

Figure 7: Ray seismograms from Figure 6 (red) overlaid by ray seismograms (black) in model M3 (AN/AN) with effects of attenuation on the reflection coefficient ignored. Full triangle indicates the position of the critical point in model M1.

Another important phenomenon, which can affect quality of synthetic seismograms computed in attenuative media is the application of either causal or non-causal attenuation, see, for example, Klimeš, (2022). In Figure 9, ray synthetic seismograms in M3 (AN/AN) model shown Figure 6 (red) computed with causal attenuation are overlaid by ray synthetic seismograms (black) calculated for the same model with non-causal attenuation. In contrast to Klimeš, (2022), we concentrate on a single SH reflected wave. Still, we can observe the phase shift of non-causal seismograms to sooner incorrect arrivals. The phase shift increases with increasing offset. The phenomenon is discussed in detail by Klimeš, (2022).

So far, we presented comparisons of synthetic seismograms. Equally valuable are comparisons of maximum spectral amplitudes. Figures 10, 11 and 12 show comparisons of ray results (black) and PS results (red) for models M1, M2 and M3, respectively. They show the well-known incorrect behaviour of the ray results in the vicinity of the critical incidence, which is sampled more densely. Specifically, one can observe increase of amplitudes to infinity from the subcritical region and slow smooth decay in the overcritical region.

In Figure 10, ray and PS amplitude curves for M1(EL/EL) model are shown. In the subcritical region, we can observe a perfect fit of both PS (red) and ray (black) amplitude curves. As expected, they start to diverge in a close vicinity of the critical point. In contrast to smooth ray amplitude curve in the overcritical region, PS curve displays

oscillations. Significant oscillations close to the critical point represent an interference of the reflected and head waves. The ray amplitudes vary smoothly in this region because the head wave is ignored in ray computations. Additional oscillations of PS amplitude curve in greater offsets are artificial. They are caused by the interference of the reflected wave with ghost waves (numerical artifacts).

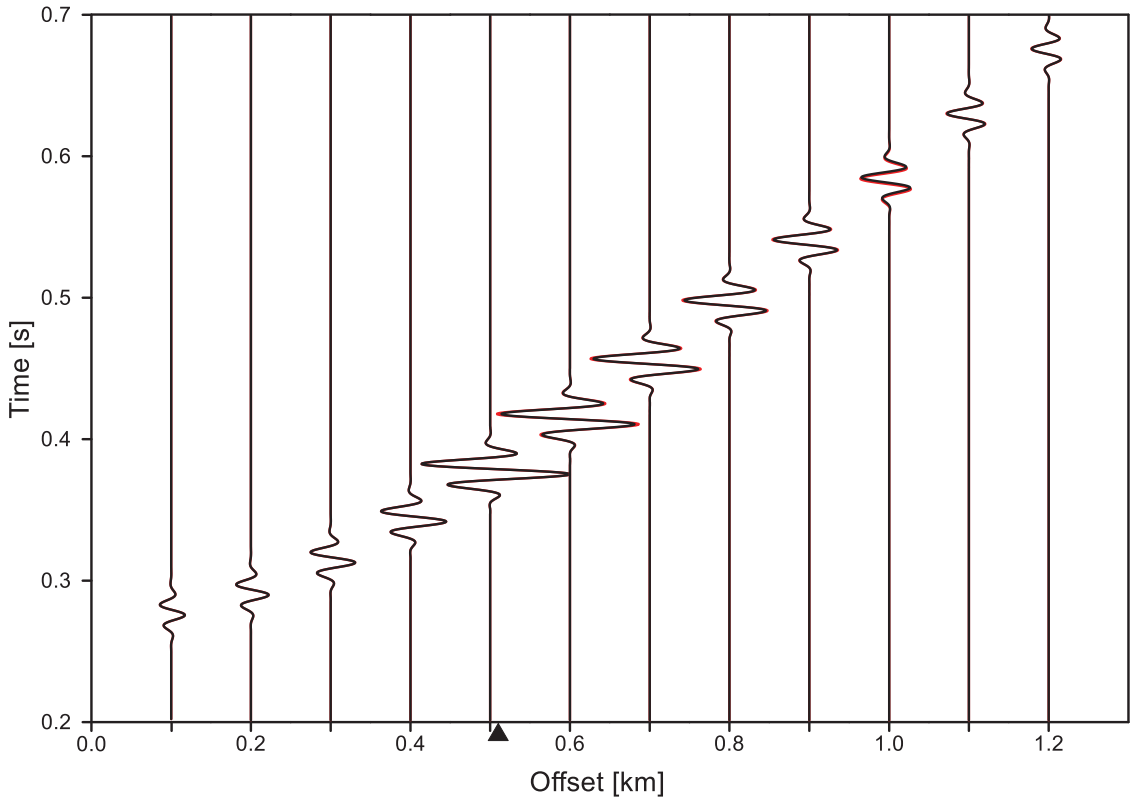

Figure 8: Ray seismograms from Figure 6 (red) overlaid by ray seismograms (black) in model M3 (AN/AN), in which the propagation vector of the transmitted wave at the reflection point in the overcritical region is not forced to point to the bottom half-space. For details, see Pšenčík et al. (2022). Full triangle indicates the position of the critical point in model M1.

The amplitude curves shown in Figure 11 correspond to model M2 (EL/AN). They reflect effects of attenuation on just the reflection coefficient. We can observe a slight decay of amplitudes and also of oscillations, especially those caused by ghost waves. But except the close vicinity of the critical point, we can observe a perfect fit of both curves.

Use of model M3 (AN/AN) leads to significantly different results presented in Figure 12. Note the dramatic change of the scale on the vertical axis with respect to Figures 10 and 11. The fit of both ray and PS amplitude curves is, however, except the critical region, even better than in models without attenuation.

Finally, in Figure 13, we show that the effects of attenuation on the reflection coefficient are negligible. The considered model is again M2. Comparing Figure 11 (effect of attenuation on the reflection coefficient included) and Figure 13 (without this effect), we can see some differences, but they concentrate to the critical region. Outside the critical

region, behaviour of both ray amplitude curves is nearly identical. Indeed, effects of attenuation on reflection can be ignored. Gajewski and Pšenčík (1992) did not make great mistake by ignoring them.

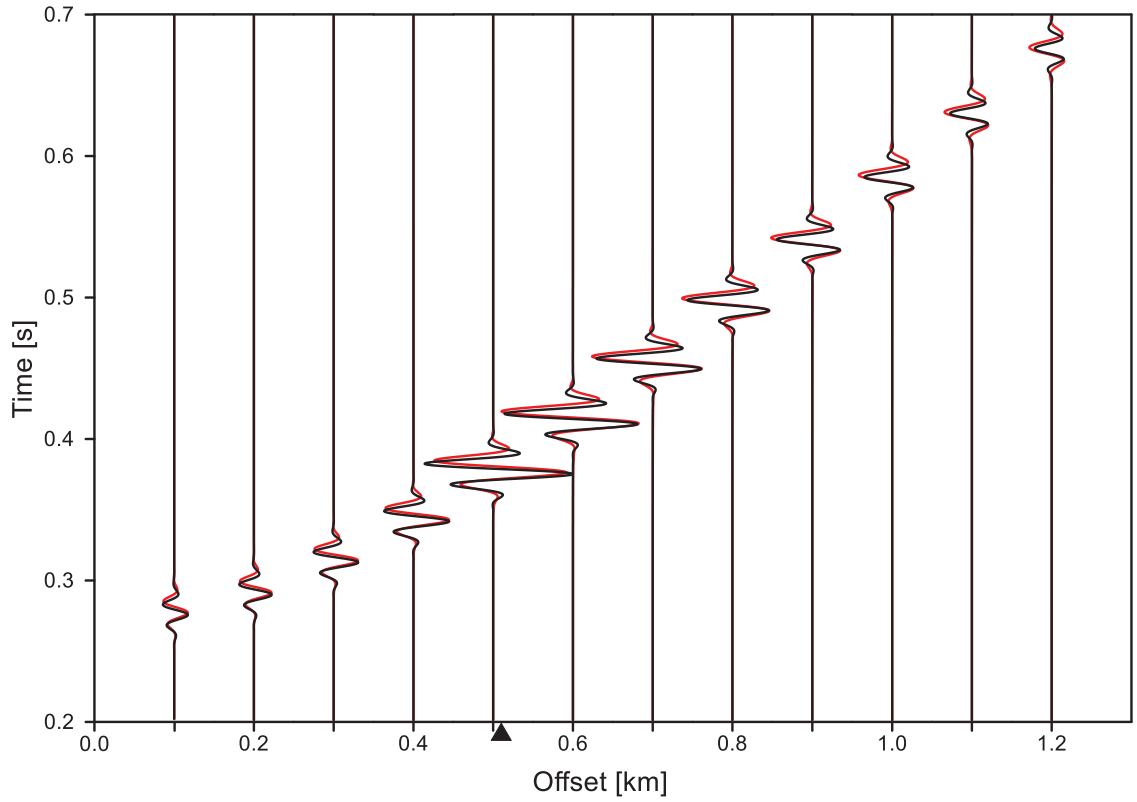

Figure 9: Ray seismograms from Figure 6 (red) overlaid by ray seismograms (black) in model M3 (AN/AN) with non-causal attenuation. Full triangle indicates the position of the critical point in model M1.

Conclusion

Comparison of ray seismograms with PS seismograms considered as an exact reference provides several interesting results. First of all, it shows that outside the critical region, the ray results fit very well the PS results. The comparison confirms previous observations that the neglection of effects of attenuation on the reflection/transmission does not lead to significant losses of accuracy of ray computations. The ray computations fail to describe properly behaviour of the wavefield in the critical region because it does not include head wave. On the other hand, ray computations do not suffer from "ghost" waves caused by numerical errors in the PS computations.

Next natural steps of the present study include tests with lower values of Q than those used in this study. Of great interest are studies of multiply reflected/transmitted waves in multilayer models. Further natural extension is to P and SV waves and, generally, to anisotropic media.

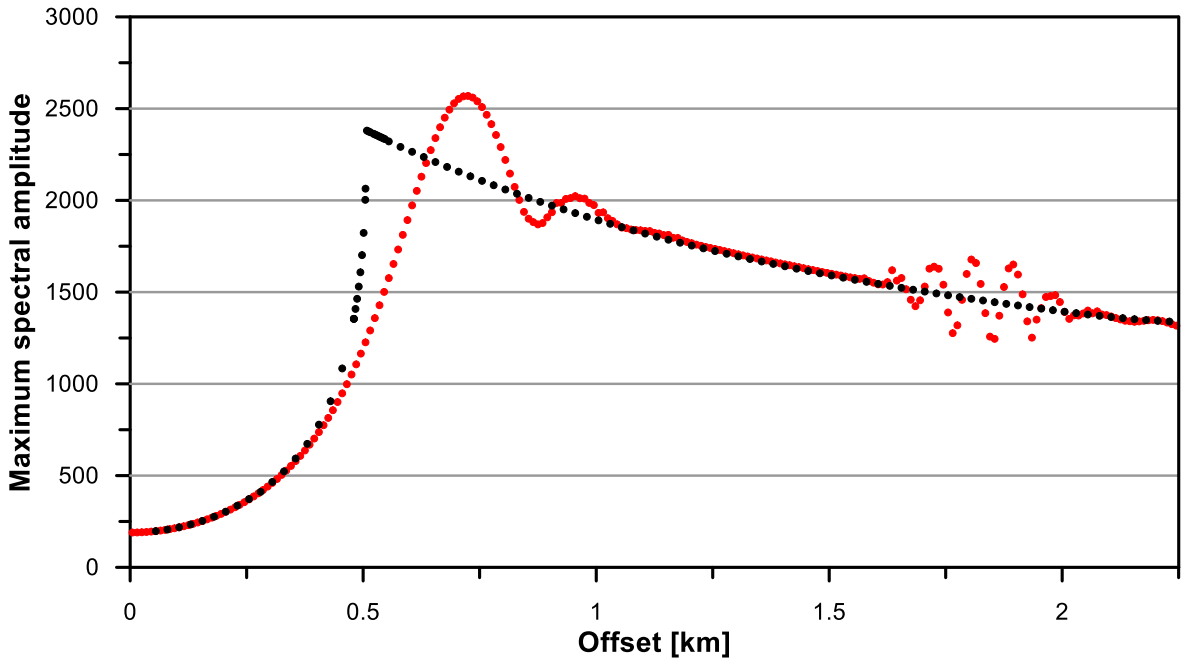

Figure 10: Maximum spectral amplitudes for model M1 calculated with the PS method (red) and by the ray method (black). Note the differences around the critical point (0.506 km) and in the overcritical region (1.5-2 km). In the former case, they are caused by ignoring head wave in ray computations, in the latter case, they are caused by numerical errors in the PS computations.

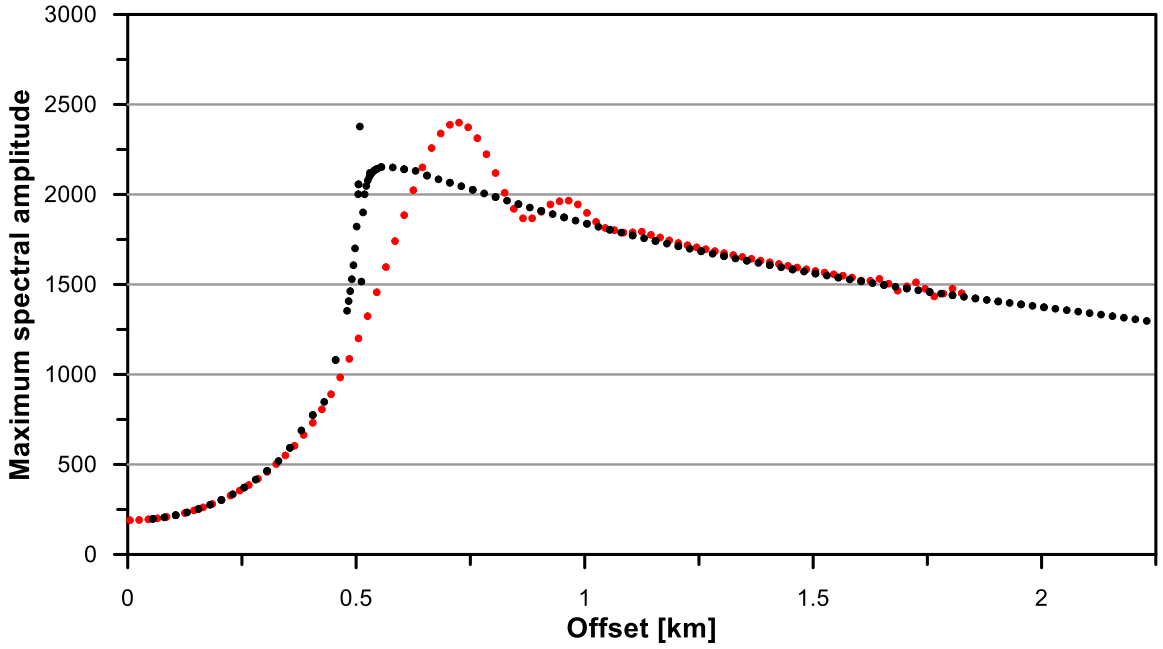

Figure 11: Maximum spectral amplitudes for model M2 calculated with the PS method (red) and by the ray method with WAC (black). Note the differences around the critical point (0.506 km) and in the overcritical region (1.5-2 km). In the former case, they are caused by ignoring head wave in ray computations, in the latter case, they are caused by numerical errors in the PS computations.

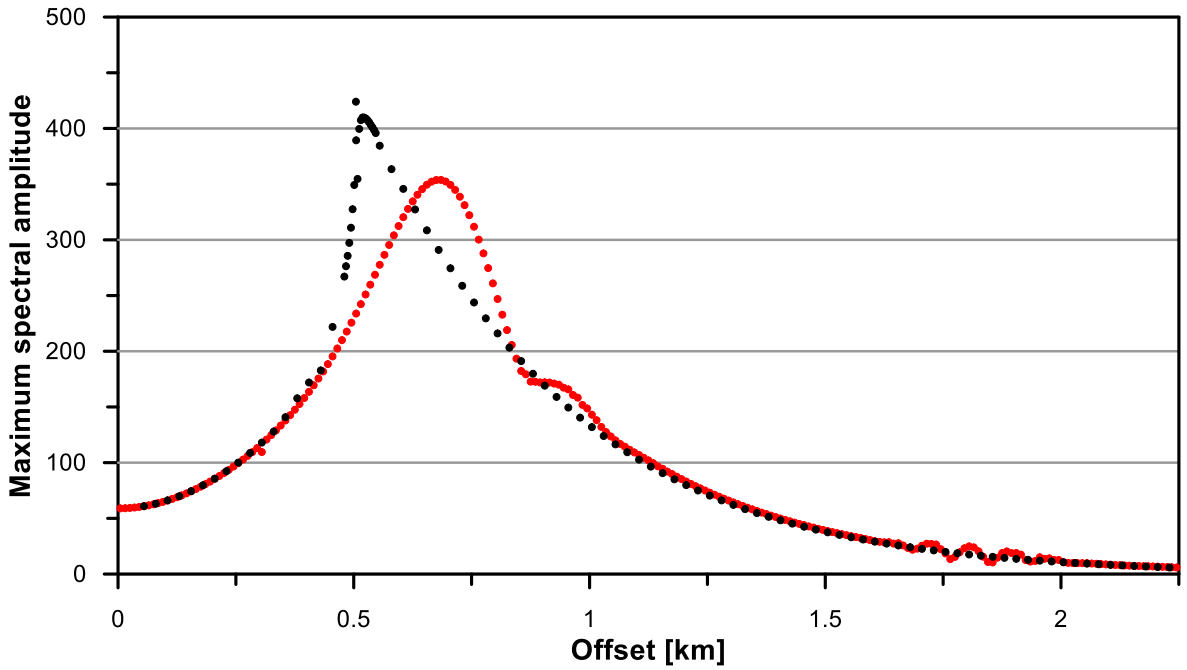

Figure 12: Maximum spectral amplitudes for model M3 calculated with the PS method (red) and by the ray method (black). Note reduced amplitude scale with respect to Figures 10 and 11.

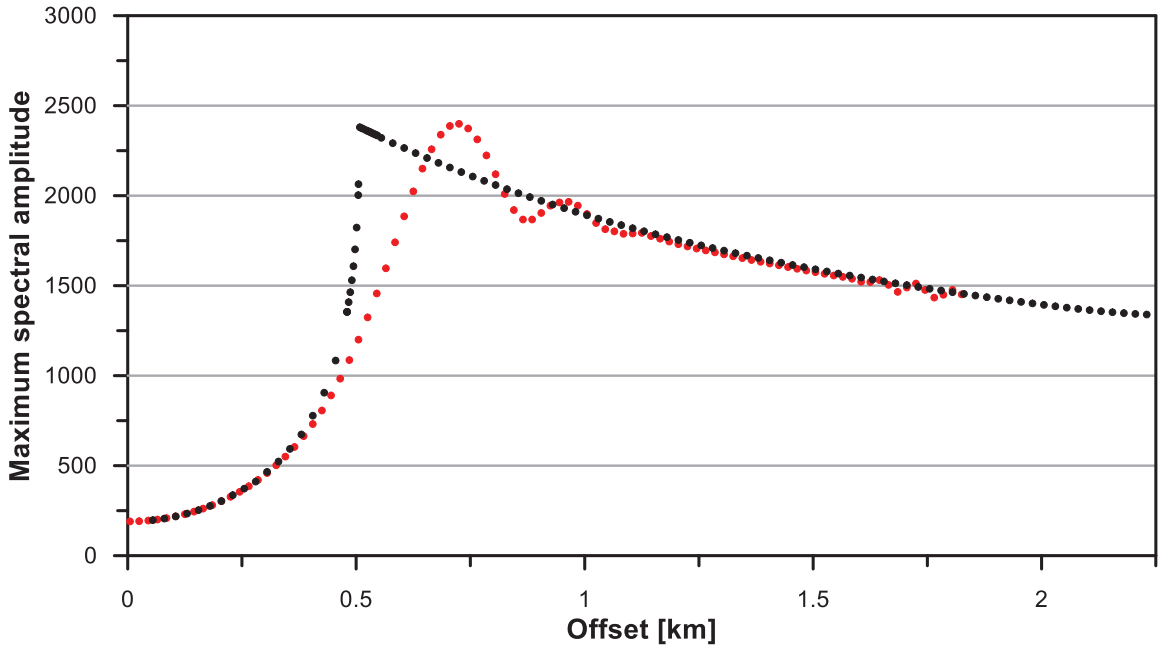

Figure 13: Maximum spectral amplitudes for model M2 calculated with the PS method (red) and by the ray method (black), in which attenuation effects on the reflection coefficient are ignored.

Acknowledgements

We thank the project "Seismic waves in complex 3-D structures" (SW3D), Research Project 20-06887S of the Grant Agency of the Czech Republic, the project SVV 260581 of the Charles University, and the research project CzechGeo/EPOS LM2015079 of the Ministry of Education, Youth and Sports of the Czech Republic for support. This study was a part of the long-term conceptual development of the Institute of Rock Structure and Mechanics CAS, RVO: 67985891.

References

Carcione, J. M., 2014. Wave fields in real media: wave propagation in anisotropic, anelastic, porous and electromagnetic media. In: Handbook of Geophysical Exploration, 3rd edn., revised and extended, Oxford.

Carcione, J. M., Gei, D., Botelho, M. A. B., Osella, A., and de la Vega, M., 2006. Fresnel reflection coefficients for GPR-AVO analysis and detection of seawater and NAPL contaminants. *Near Surf. Geophys.*, **4**, 253-263.

Carcione, J. M., and Helle H. B., 2004. On the physics and simulation of wave propagation at the ocean bottom. *Geophysics*, **69**, 825–839.

Červený, V., 2001. Seismic Ray Theory, Cambridge Univ. Press, Cambridge.

Červený, V., and Pšenčík, I., 1984. Documentation of earthquake algorithms. SEIS83 - Numerical modeling of seismic wave fields in 2-D laterally varying layered structures by the ray method. E.R.Engdahl edit., Report SE-35, Boulder: 36–40.

Gajewski D., and Pšenčík, I., 1992. Vector wave fields for weakly attenuating anisotropic media by the ray method. *Geophysics*, **57**, 27–38.

Klimeš, L., 2021. Comparison of ray-theory synthetic seismograms with finite differences in 2D velocity model UNCONFORMITY. *J. Seis. Explor.*, **30**, 271–279.

Klimeš, L., 2022. Effects of causal and noncausal attenuation in 2-D velocity model UNCONFORMITY. *J. appl. Geophys.*, submitted.

Kravtsov, Yu. A., Orlov, Yu I., 1990. Geometrical optics of inhomogeneous media. Springer, New York.

Moczo P., Bard P.-Y., Pšenčík, I. 1987. Seismic response of 2-D absorbing structures by the ray method. *J. Geophys.*, **62**, 38–49.

Müller, G., 1983. Rheological properties and velocity dispersion of a medium with power-law dependence of Q on frequency, *J.Geophys.*, **54**, 20–29.

Pšenčík, I., Wcisło, M., and Daley, P.F., 2022. SH plane-wave reflection/transmission coefficients in isotropic, weakly attenuating media. *Journal of Seismology*, doi.org/10.1007/s10950-021-10052-x.

Sidler, R., and Carcione, J. M., 2007. Wave reflection at an anelastic transversely isotropic ocean bottom. *Geophysics*, **72**, SM139–SM146.

Sidler, R., Carcione, J. M., and Holliger, K., 2008. On the evaluation of the plane-wave reflection coefficients in anelastic media. *Geophys. J. Internat.*, **175**, 94–102.

Ursin, B., Carcione, J. M., and Gei, D., 2017. A physical solution for plane SH waves in anelastic media. *Geophys. J. Internat.*, **209**, 661–671.